Journal of Zhejiang University SCIENCE A
ISSN 1673-565X (Print); ISSN 1862-1775 (Online)
www.zju.edu.cn/jzus; www.springerlink.com
E-mail: jzus@zju.edu.cn

Enhanced control of DFIG-used back-to-back PWM VSC under unbalanced grid voltage conditions*

HU Jia-bing†, HE Yi-kang†‡, NIAN Heng

(*School of Electrical Engineering, Zhejiang University, Hangzhou 310027, China*)

†E-mail: emec_zju@zju.edu.cn; ykhe@zju.edu.cn

Received Mar. 2, 2007; revision accepted May 19, 2007

Abstract: This paper presents a unified positive- and negative-sequence dual-*dq* dynamic model of wind-turbine driven doubly-fed induction generator (DFIG) under unbalanced grid voltage conditions. Strategies for enhanced control and operation of a DFIG-used back-to-back (BTB) PWM voltage source converter (VSC) are proposed. The modified control design for the grid-side converter in the stationary $\alpha\beta$ frames diminishes the amplitude of DC-link voltage ripples of twice the grid frequency, and the two proposed control targets for the rotor-side converter are alternatively achieved, which, as a result, improve the fault-ride through (FRT) capability of the DFIG based wind power generation systems during unbalanced network supply. A complete unbalanced control scheme with both grid- and rotor-side converters included is designed. Finally, simulation was carried out on a 1.5 MW wind-turbine driven DFIG system and the validity of the developed unified model and the feasibility of the proposed control strategies are all confirmed by the simulated results.

Key words: Unbalanced grid voltage, Doubly-fed induction generator (DFIG), Back-to-back (BTB), Fault-ride through (FRT), Voltage source converter (VSC)

doi:10.1631/jzus.2007.A1330 **Document code:** A **CLC number:** TM315; TM614

INTRODUCTION

The forced-commutated PWM voltage source converter (VSC) has been increasingly employed as one of the building blocks in the electric power systems including FACTS controllers and HVDC systems, and for renewable energy conversion systems such as wind-energy and photovoltaic solar energy generation systems. In particular, as in wind-energy developments, in order to overcome the problems associated with the traditional fixed-speed systems and to maximize the wind-energy capture, variable-speed wind turbines based on doubly-fed induction generator (DFIG) equipped with a back-to-back (BTB) PWM VSC, including grid- and rotor-side converters connected between the grid and the DFIG rotor, will be employed in many new wind farms. During balanced grid conditions, the rotor-side converter controls the DFIG stator output active power as well as reactive power with control system usually defined in the stator-flux oriented (SFO) synchronous reference frame. Meanwhile, the grid-side converter maintains a constant DC-link voltage with the controller usually defined in the synchronous reference frame fixed to the stator voltage. The characteristics of such scheme under normal operation conditions, in which both converters are vector-controlled, could be categorized as follows (Pena *et al*., 1996): (1) independent control capability of stator output active and reactive powers with bi-directional power flow; (2) low distortion of stator, rotor and supply currents and high-quality DC-link voltage with a relatively small filter capacitor; (3) control of the displacement factor between the voltage and the currents for grid-side converter; (4) typical converter rating at around 30% of the generator rating for a given rotor speed range of 0.75~1.25 p.u.

‡ Corresponding author

* Project (No. 50577056) supported by the National Natural Science Foundation of China

These advantages cannot be entirely achieved during unbalanced grid voltage conditions, which, however, are common in power systems, especially for weak AC systems.

Recently, a number of studies have been carried out to examine the fault-ride through (FRT) capability of the DFIG system during network disturbance (Tapia *et al*., 2003; Morren *et al*., 2003; Sun *et al*., 2005; Morren and de Haan, 2005; Petersson *et al*., 2005). Whereas for all the work reported, the network voltage was assumed to be symmetrical. However, in practice, asymmetric faults occur more frequently than symmetric ones. For a DFIG system, if the voltage unbalance is not considered in the control system, the stator current could be highly unbalanced even with a small unbalanced stator voltage. The unbalanced currents create unequal heating among stator windings and torque pulsation in the generator. A wind-turbine driven DFIG without unbalancing voltage control considered might have to be disconnected from the network during network voltage unbalance (Idsoe Nass *et al*., 2002). On the other hand, the emerging grid codes require the wind farm to withstand the negative-sequence currents that occur during phase-to-phase faults on the transmission or distribution system without disconnection (National Grid Transco, 2004). In addition, the wind farm should be able to withstand a maximum value of phase voltage at the small steady-state unbalance of 2% and large transient unbalance of 5% without tripping (National Grid Transco, 2004). Nevertheless, the detailed impacts of unbalanced supply on the operation of DFIG and the associated converters are still largely unknown.

Existing literature (Stankovic and Lipo, 2001; Xu *et al*., 2005; Yazdani and Iravani, 2006) report extensive studies on grid-connected PWM VSC control strategies to minimize and even to eliminate the harmonics in the input current and the ripples of twice the grid frequency in the DC-link voltage. It was concluded that the control schemes, conducted in both positive- and negative-synchronously rotating reference frames, have their inherent defects, including the limited bandwidth of current-control loops due to the decomposition of positive- and negative-sequence components by using low-pass or notch filter. Besides, the converter was assumed to be loaded with a purely resistive impedance, which is an erroneous approximation in DFIG-used BTB PWM VSC, especially during grid disturbance. Yazdani and Iravani (2006) presented a unified dynamic model for BTB VSC-based systems and approved its application to a variable-speed directly-driven wind-power generation system under unbalanced grid conditions. Whenas, the situation becomes more complicated in the wind-turbine driven DFIG systems under unbalanced grid voltage due to the existing electro-mechanical interactions, limited rotor converter rating and oscillating power flow exchange between the generator rotor and the rotor-side converter. It has never been reported in previous works on how the strategies should be adopted in order to provide DFIG systems with enhanced performance, and how the strategy is implemented on the machine and especially on the associated converter control system to meet the overall operational targets.

This paper presents a unified positive- and negative-sequence dual-dq dynamic model for a wind-turbine driven DFIG under unbalanced grid voltage conditions. Strategies for the enhanced control and operation of a DFIG-used BTB PWM VSC is proposed, which provides unbalanced FRT capability for the DFIG based wind power generation systems during unbalanced network supply voltage. A complete unbalanced control scheme for both grid- and rotor-side converters is designed. Finally, simulation was conducted on a 1.5 MW wind-turbine driven DFIG system. The validity of the developed unified model and the feasibility of the proposed control strategies are confirmed by the results.

MATHEMATICAL MODEL OF DFIG

Fig.1 shows the spatial relationship between the stationary $\alpha\beta$ reference frame, dq^+ and dq^- reference frames rotating at the angular speed of ω_s and $-\omega_s$, respectively. According to Fig.1, the transformation between $\alpha\beta$, dq^+ and dq^- reference frames are given by

$$\boldsymbol{F}_{dq}^{+}=\boldsymbol{F}_{\alpha\beta}\mathrm{e}^{-\mathrm{j}\omega_s t},\ \ \boldsymbol{F}_{dq}^{-}=\boldsymbol{F}_{\alpha\beta}\mathrm{e}^{\mathrm{j}\omega_s t}, \tag{1a}$$

$$\boldsymbol{F}_{dq}^{+}=\boldsymbol{F}_{dq}^{-}\mathrm{e}^{-\mathrm{j}2\omega_s t},\ \ \boldsymbol{F}_{dq}^{-}=\boldsymbol{F}_{dq}^{+}\mathrm{e}^{\mathrm{j}2\omega_s t}, \tag{1b}$$

where superscripts +, − represent the positive- and negative-rotating reference frames, respectively.

The equivalent circuit of DFIG in the dq^+ reference frame is shown in Fig.2.

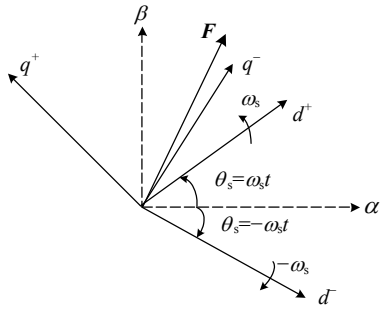

Fig.1 Relationship between the $\alpha\beta$, dq^+ and dq^- reference frames

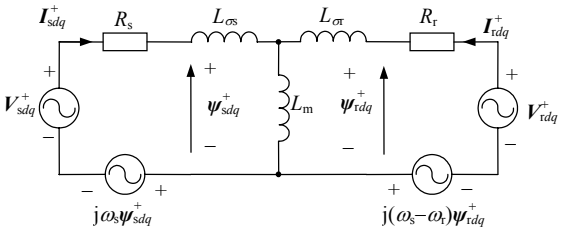

Fig.2 T-representation of the DFIG equivalent circuit in the positive-reference frame rotating at the speed of ω_s

According to Fig.2, the stator and rotor flux $\boldsymbol{\psi}_{sdq}^+$ and $\boldsymbol{\psi}_{rdq}^+$ are represented respectively by

$$\boldsymbol{\psi}_{sdq}^+ = L_s\boldsymbol{I}_{sdq}^+ + L_m\boldsymbol{I}_{rdq}^+, \tag{2}$$

$$\boldsymbol{\psi}_{rdq}^+ = L_m\boldsymbol{I}_{sdq}^+ + L_r\boldsymbol{I}_{rdq}^+. \tag{3}$$

From Fig.2, the stator and rotor voltages $\boldsymbol{V}_{sdq}^+$ and $\boldsymbol{V}_{rdq}^+$ in the dq^+ reference frame can be expressed as

$$\boldsymbol{V}_{sdq}^+ = R_s\boldsymbol{I}_{sdq}^+ + \frac{\mathrm{d}\boldsymbol{\psi}_{sdq}^+}{\mathrm{d}t} + \mathrm{j}\omega_s\boldsymbol{\psi}_{sdq}^+, \tag{4}$$

$$\boldsymbol{V}_{rdq}^+ = R_r\boldsymbol{I}_{rdq}^+ + \frac{\mathrm{d}\boldsymbol{\psi}_{rdq}^+}{\mathrm{d}t} + \mathrm{j}\omega_{slip+}\boldsymbol{\psi}_{rdq}^+, \tag{5}$$

where, R_s and R_r are stator resistance and rotor resistance, respectively; $L_s=L_{\sigma s}+L_m$ and $L_r=L_{\sigma r}+L_m$ are total self-inductance of stator and rotor windings respectively; $L_{\sigma s}$, $L_{\sigma r}$ and L_m are stator and rotor leakage inductances and mutual inductance, respectively; ω_s is synchronous angular speed; ω_r is rotor angular speed; $\omega_{slip+}=\omega_s-\omega_r$ is slip angular speed.

According to Eq.(1) and Fig.1, the stator and rotor current, voltage and flux vectors can be expressed in terms of positive- and negative-sequence components in the positive- and negative-synchronously rotating frames, respectively as

$$\begin{cases}
\boldsymbol{V}_{sdq}^+ = \boldsymbol{V}_{sdq+}^+ + \boldsymbol{V}_{sdq-}^+ = \boldsymbol{V}_{sdq+}^+ + \boldsymbol{V}_{sdq-}^-\mathrm{e}^{-\mathrm{j}2\omega_s t},\\
\boldsymbol{I}_{sdq}^+ = \boldsymbol{I}_{sdq+}^+ + \boldsymbol{I}_{sdq-}^+ = \boldsymbol{I}_{sdq+}^+ + \boldsymbol{I}_{sdq-}^-\mathrm{e}^{-\mathrm{j}2\omega_s t},\\
\boldsymbol{\psi}_{sdq}^+ = \boldsymbol{\psi}_{sdq+}^+ + \boldsymbol{\psi}_{sdq-}^+ = \boldsymbol{\psi}_{sdq+}^+ + \boldsymbol{\psi}_{sdq-}^-\mathrm{e}^{-\mathrm{j}2\omega_s t},\\
\boldsymbol{V}_{rdq}^+ = \boldsymbol{V}_{rdq+}^+ + \boldsymbol{V}_{rdq-}^+ = \boldsymbol{V}_{rdq+}^+ + \boldsymbol{V}_{rdq-}^-\mathrm{e}^{-\mathrm{j}2\omega_s t},\\
\boldsymbol{I}_{rdq}^+ = \boldsymbol{I}_{rdq+}^+ + \boldsymbol{I}_{rdq-}^+ = \boldsymbol{I}_{rdq+}^+ + \boldsymbol{I}_{rdq-}^-\mathrm{e}^{-\mathrm{j}2\omega_s t},\\
\boldsymbol{\psi}_{rdq}^+ = \boldsymbol{\psi}_{rdq+}^+ + \boldsymbol{\psi}_{rdq-}^+ = \boldsymbol{\psi}_{rdq+}^+ + \boldsymbol{\psi}_{rdq-}^-\mathrm{e}^{-\mathrm{j}2\omega_s t},
\end{cases} \tag{6}$$

where subscripts +, − represent positive- and negative-sequence components respectively.

According to Eqs.(2) and (3), the rotor flux and stator current can be calculated as

$$\boldsymbol{\psi}_{rdq}^+ = L_m\boldsymbol{\psi}_{sdq}^+ / L_s + \sigma L_r\boldsymbol{I}_{rdq}^+, \tag{7}$$

$$\boldsymbol{I}_{sdq}^+ = (\boldsymbol{\psi}_{sdq}^+ - L_m\boldsymbol{I}_{rdq}^+)/L_s, \tag{8}$$

where $\sigma=1-L_m^2/(L_sL_r)$ is the leakage factor.

Substituting Eq.(7) into Eq.(5) yields the rotor voltage in the dq^+ reference frame as

$$\begin{aligned}
\boldsymbol{V}_r^+ &= R_r\boldsymbol{I}_r^+ + \frac{\mathrm{d}}{\mathrm{d}t}\left(\frac{L_m}{L_s}\boldsymbol{\psi}_s^+ + \sigma L_r\boldsymbol{I}_r^+\right) + \mathrm{j}\omega_{slip+}\left(\frac{L_m}{L_s}\boldsymbol{\psi}_s^+ + \sigma L_r\boldsymbol{I}_r^+\right)\\
&= R_r\boldsymbol{I}_r^+ + \sigma L_r\frac{\mathrm{d}\boldsymbol{I}_r^+}{\mathrm{d}t} + \frac{L_m}{L_s}\frac{\mathrm{d}\boldsymbol{\psi}_s^+}{\mathrm{d}t} + \mathrm{j}\omega_{slip+}\left(\frac{L_m}{L_s}\boldsymbol{\psi}_s^+ + \sigma L_r\boldsymbol{I}_r^+\right).
\end{aligned} \tag{9}$$

The equivalent DFIG model in the dq^- reference frame is similar to that in the dq^+ frame except for replacing the superscript + in Eqs.(2)~(5) and Eqs.(7)~(9) with −, and the ω_{slip+} in Eqs.(5) and (9) with $\omega_{slip-}=-\omega_s-\omega_r$.

According to Eq.(6), Eq.(5) could be rewritten as

$$\begin{aligned}
\boldsymbol{V}_{rdq}^+ &= R_r\boldsymbol{I}_{rdq}^+ + \frac{\mathrm{d}\boldsymbol{\psi}_{rdq}^+}{\mathrm{d}t} + \mathrm{j}\omega_{slip+}\boldsymbol{\psi}_{rdq}^+ \approx \frac{\mathrm{d}\boldsymbol{\psi}_{rdq}^+}{\mathrm{d}t} + \mathrm{j}\omega_{slip+}\boldsymbol{\psi}_{rdq}^+\\
&= \frac{\mathrm{d}}{\mathrm{d}t}(\boldsymbol{\psi}_{rdq+}^+ + \boldsymbol{\psi}_{rdq-}^-\mathrm{e}^{-\mathrm{j}2\omega_s t}) + \mathrm{j}\omega_{slip+}(\boldsymbol{\psi}_{rdq+}^+ + \boldsymbol{\psi}_{rdq-}^-\mathrm{e}^{-\mathrm{j}2\omega_s t})\\
&= -\mathrm{j}2\omega_s\boldsymbol{\psi}_{sdq-}^-\mathrm{e}^{-\mathrm{j}2\omega_s t} + \mathrm{j}\omega_{slip+}(\boldsymbol{\psi}_{rdq+}^+ + \boldsymbol{\psi}_{rdq-}^-\mathrm{e}^{-\mathrm{j}2\omega_s t})\\
&= \mathrm{j}(\omega_{slip+}\boldsymbol{\psi}_{rdq+}^+ + \omega_{slip-}\boldsymbol{\psi}_{rdq-}^-\mathrm{e}^{-\mathrm{j}2\omega_s t}).
\end{aligned} \tag{10}$$

Similar to that under balanced grid voltage supply, the stator output instantaneous active and reactive powers under unbalanced network condition could be expressed as

$$\begin{aligned} P_{\mathrm{s}}+\mathrm{j}Q_{\mathrm{s}} &= -3\boldsymbol{V}_{sdq}^{+}\hat{\boldsymbol{I}}_{sdq}^{+}/2 \\ &=[P_{\mathrm{s}0}+P_{\mathrm{s}\sin 2}\sin(2\omega_{\mathrm{s}}t)+P_{\mathrm{s}\cos 2}\cos(2\omega_{\mathrm{s}}t)] \\ &\quad +\mathrm{j}[Q_{\mathrm{s}0}+Q_{\mathrm{s}\sin 2}\sin(2\omega_{\mathrm{s}}t)+Q_{\mathrm{s}\cos 2}\cos(2\omega_{\mathrm{s}}t)], \end{aligned} \tag{11}$$

where $\hat{\boldsymbol{I}}_{sdq}^{+}$ is the conjugated space vector of $\boldsymbol{I}_{sdq}^{+}$; $P_{\mathrm{s}0}$, $P_{\mathrm{s}\sin 2}$ and $P_{\mathrm{s}\cos 2}$ are the DC average, cosine and sine terms of twice the line frequency contained in the instantaneous stator output active power, respectively; $Q_{\mathrm{s}0}$, $Q_{\mathrm{s}\sin 2}$ and $Q_{\mathrm{s}\cos 2}$ are the DC average, cosine and sine terms of twice the line frequency contained in the instantaneous stator output reactive power, respectively.

Rearranging Eq.(11) as a matrix product form yields

$$\begin{aligned} \begin{bmatrix} P_{\mathrm{s}0} \\ Q_{\mathrm{s}0} \\ P_{\mathrm{s}\sin 2} \\ P_{\mathrm{s}\cos 2} \\ Q_{\mathrm{s}\sin 2} \\ Q_{\mathrm{s}\cos 2} \end{bmatrix} &= -\frac{3}{2}\frac{1}{L_{\mathrm{s}}}\begin{bmatrix} V_{sd+}^{+} & V_{sq+}^{+} & V_{sd-}^{-} & V_{sq-}^{-} \\ V_{sq+}^{+} & -V_{sd+}^{+} & V_{sq-}^{-} & -V_{sd-}^{-} \\ V_{sq-}^{-} & -V_{sd-}^{-} & -V_{sq+}^{+} & V_{sd+}^{+} \\ V_{sd-}^{-} & V_{sq-}^{-} & V_{sd+}^{+} & V_{sq+}^{+} \\ -V_{sd-}^{-} & -V_{sq-}^{-} & V_{sq+}^{+} & V_{sd+}^{+} \\ V_{sq-}^{-} & -V_{sd-}^{-} & V_{sq+}^{+} & -V_{sd+}^{+} \end{bmatrix}\begin{bmatrix} \psi_{sd+}^{+} \\ \psi_{sq+}^{+} \\ \psi_{sd-}^{-} \\ \psi_{sq-}^{-} \end{bmatrix} \\ &\quad +\frac{3}{2}\frac{L_{\mathrm{m}}}{L_{\mathrm{s}}}\begin{bmatrix} V_{sd+}^{+} & V_{sq+}^{+} & V_{sd-}^{-} & V_{sq-}^{-} \\ V_{sq+}^{+} & -V_{sd+}^{+} & V_{sq-}^{-} & -V_{sd-}^{-} \\ V_{sq-}^{-} & -V_{sd-}^{-} & -V_{sq+}^{+} & V_{sd+}^{+} \\ V_{sd-}^{-} & V_{sq-}^{-} & V_{sd+}^{+} & V_{sq+}^{+} \\ -V_{sd-}^{-} & -V_{sq-}^{-} & V_{sq+}^{+} & V_{sd+}^{+} \\ V_{sq-}^{-} & -V_{sd-}^{-} & V_{sq+}^{+} & -V_{sd+}^{+} \end{bmatrix}\begin{bmatrix} I_{rd+}^{+} \\ I_{rq+}^{+} \\ I_{rd-}^{-} \\ I_{rq-}^{-} \end{bmatrix}. \end{aligned} \tag{12}$$

According to Eq.(10), the rotor output instantaneous active and reactive powers could be represented as

$$\begin{aligned} P_{\mathrm{r}}+\mathrm{j}Q_{\mathrm{r}} &= -3\boldsymbol{V}_{rdq}^{+}\hat{\boldsymbol{I}}_{rdq}^{+}/2 \\ &= -3\mathrm{j}(\omega_{\mathrm{slip}+}\boldsymbol{\psi}_{rdq+}^{+}+\omega_{\mathrm{slip}-}\boldsymbol{\psi}_{rdq-}^{-}\mathrm{e}^{-\mathrm{j}2\omega_{\mathrm{s}}t})(\hat{\boldsymbol{I}}_{rdq+}^{+}+\hat{\boldsymbol{I}}_{rdq-}^{-}\mathrm{e}^{\mathrm{j}2\omega_{\mathrm{s}}t})/2 \\ &=[P_{\mathrm{r}0}+P_{\mathrm{r}\sin 2}\sin(2\omega_{\mathrm{s}}t)+P_{\mathrm{r}\cos 2}\cos(2\omega_{\mathrm{s}}t)] \\ &\quad +\mathrm{j}[Q_{\mathrm{r}0}+Q_{\mathrm{r}\sin 2}\sin(2\omega_{\mathrm{s}}t)+Q_{\mathrm{r}\cos 2}\cos(2\omega_{\mathrm{s}}t)], \end{aligned} \tag{13}$$

where $\hat{\boldsymbol{I}}_{rdq}^{+}$ is the conjugated space vector of $\hat{\boldsymbol{I}}_{rdq}^{+}$; $P_{\mathrm{r}0}$, $P_{\mathrm{r}\sin 2}$ and $P_{\mathrm{r}\cos 2}$ are the DC average, cosine and sine terms of twice the line frequency contained in the instantaneous rotor active power, respectively; $Q_{\mathrm{r}0}$, $Q_{\mathrm{r}\sin 2}$ and $Q_{\mathrm{r}\cos 2}$ are the DC average, cosine and sine terms of twice the line frequency contained in the instantaneous rotor reactive power, respectively.

Similar to Eq.(11), Eq.(13) can be rearranged as

$$\begin{bmatrix} P_{\mathrm{r}0} \\ Q_{\mathrm{r}0} \\ P_{\mathrm{r}\sin 2} \\ P_{\mathrm{r}\cos 2} \\ Q_{\mathrm{r}\sin 2} \\ Q_{\mathrm{r}\cos 2} \end{bmatrix} = \frac{3}{2}\begin{bmatrix} \omega_{\mathrm{slip}+}\boldsymbol{M}_{11} & \omega_{\mathrm{slip}-}\boldsymbol{M}_{12} \\ \omega_{\mathrm{slip}-}\boldsymbol{M}_{12} & \omega_{\mathrm{slip}+}\boldsymbol{M}_{22} \\ \omega_{\mathrm{slip}-}\boldsymbol{M}_{21} & \omega_{\mathrm{slip}+}\boldsymbol{M}_{11} \end{bmatrix}\begin{bmatrix} I_{rd+}^{+} \\ I_{rq+}^{+} \\ I_{rd-}^{-} \\ I_{rq-}^{-} \end{bmatrix}, \tag{14}$$

where,

$$\boldsymbol{M}_{11}=\begin{bmatrix} \psi_{rq+}^{+} & -\psi_{rd+}^{+} \\ -\psi_{rd+}^{+} & -\psi_{rq+}^{+} \end{bmatrix},\ \boldsymbol{M}_{12}=\begin{bmatrix} \psi_{rq-}^{-} & -\psi_{rd-}^{-} \\ -\psi_{rd-}^{-} & -\psi_{rq-}^{-} \end{bmatrix},$$

$$\boldsymbol{M}_{21}=\begin{bmatrix} -\psi_{rq-}^{-} & \psi_{rd-}^{-} \\ -\psi_{rd-}^{-} & -\psi_{rq-}^{-} \end{bmatrix},\ \boldsymbol{M}_{22}=\begin{bmatrix} \psi_{rq+}^{+} & -\psi_{rd+}^{+} \\ \psi_{rd+}^{+} & \psi_{rq+}^{+} \end{bmatrix}.$$

CONTROL DESIGN

In this section, a new control design for the grid-side PWM VSC to minimize the DC-link voltage ripples of twice the grid frequency will be proposed under unbalanced network supply firstly. Consequently, two alternatively improved control strategies for rotor-side PWM VSC are provided. Finally, a complete unbalanced control scheme for the wind-turbine driven DFIG system with both grid- and rotor-side converters included is constructed.

Grid-side VSC control design

As shown in Fig.3, the grid-side converter of the DFIG-used BTB PWM VSC plays the role of a boost rectifier at the sub-synchronous speed and maintains a constant DC-link voltage at the full speed range of operation. Under unbalanced grid voltage conditions, its behavior can be depicted in the dq^{+} and dq^{-} reference frames as (Stankovic and Lipo, 2001)

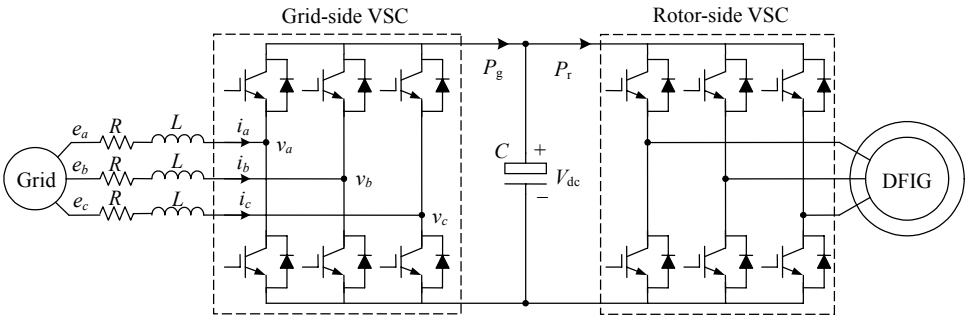

Fig.3 Schematic diagram of a BTB VSC in the wind-turbine driven DFIG system

$$\begin{cases} \boldsymbol{E}^{+}_{dq+} = L\dfrac{\mathrm{d}\boldsymbol{I}^{+}_{dq+}}{\mathrm{d}t} + R\boldsymbol{I}^{+}_{dq+} + \mathrm{j}\omega_{\mathrm{s}}L\boldsymbol{I}^{+}_{dq+} + \boldsymbol{V}^{+}_{dq+}, \\ \boldsymbol{E}^{-}_{dq-} = L\dfrac{\mathrm{d}\boldsymbol{I}^{-}_{dq-}}{\mathrm{d}t} + R\boldsymbol{I}^{-}_{dq-} - \mathrm{j}\omega_{\mathrm{s}}L\boldsymbol{I}^{-}_{dq-} + \boldsymbol{V}^{-}_{dq-}. \end{cases} \tag{15}$$

The instantaneous active and reactive powers at the input ends of the grid-side VSC can be expressed by

$$\begin{cases} P_{ac} = P_0 + P_{\mathrm{c}2}\cos(2\omega_{\mathrm{s}}t) + P_{\mathrm{s}2}\sin(2\omega_{\mathrm{s}}t), \\ Q_{ac} = Q_0 + Q_{\mathrm{c}2}\cos(2\omega_{\mathrm{s}}t) + Q_{\mathrm{s}2}\sin(2\omega_{\mathrm{s}}t), \end{cases} \tag{16a}$$

where

$$\begin{bmatrix} P_0 \\ Q_0 \\ P_{\mathrm{c}2} \\ P_{\mathrm{s}2} \\ Q_{\mathrm{c}2} \\ Q_{\mathrm{s}2} \end{bmatrix} = \frac{3}{2}\begin{bmatrix} V^{+}_{d+} & V^{+}_{q+} & V^{-}_{d-} & V^{-}_{q-} \\ V^{+}_{q+} & -V^{+}_{d+} & V^{-}_{q-} & -V^{-}_{d-} \\ V^{-}_{d-} & V^{-}_{q-} & V^{+}_{d+} & V^{+}_{q+} \\ V^{-}_{q-} & -V^{-}_{d-} & -V^{+}_{q+} & V^{+}_{d+} \\ V^{-}_{q-} & -V^{-}_{d-} & V^{+}_{q+} & -V^{+}_{d+} \\ -V^{-}_{d-} & -V^{-}_{q-} & V^{+}_{d+} & V^{+}_{q+} \end{bmatrix}\begin{bmatrix} I^{+}_{d+} \\ I^{+}_{q+} \\ I^{-}_{d-} \\ I^{-}_{q-} \end{bmatrix}. \tag{16b}$$

Therefore, by using the power-balancing equation, the DC side equation under unbalanced conditions can be expressed as

$$P_{\mathrm{g}} = P_{\mathrm{ac}} = C\frac{\mathrm{d}V_{\mathrm{dc}}}{\mathrm{d}t} + P_{\mathrm{r}}, \tag{17}$$

where P_{r} and P_{g} are the instantaneous active powers flowing through rotor- and grid-side converters, respectively.

To eliminate the DC-link voltage ripples during grid-voltage unbalance with the traditional control strategy (Stankovic and Lipo, 2001), the converter was assumed to be loaded with a purely resistive impedance, which is effective for keeping the DC-link voltage flat and for obtaining the current references by setting $P_{\mathrm{c}2}$=$P_{\mathrm{s}2}$=0. However, with regard to DFIG-used grid-side VSC, it is not reasonable yet to still employ the traditional control scheme since the load is a VSC-supplied DFIG rotor with power-flow oscillating under unbalanced grid voltage, which can be observed from Eq.(13), rather than a resistive impedance.

Therefore, a modified control strategy for minimizing the DC-link voltage ripples should be designed. As $P_{\mathrm{s}2}$ and $P_{\mathrm{c}2}$ are assumed to be the cosine and sine terms of rotor power $P_{\mathrm{r\,sin}2}$ and $P_{\mathrm{r\,cos}2}$, respectively, the current references can be figured out as

$$\begin{bmatrix} I^{+*}_{d+} \\ I^{+*}_{q+} \\ I^{-*}_{d-} \\ I^{-*}_{q-} \end{bmatrix} = \frac{2}{3}\begin{bmatrix} V^{+}_{d+} & V^{+}_{q+} & V^{-}_{d-} & V^{-}_{q-} \\ V^{+}_{q+} & -V^{+}_{d+} & V^{-}_{q-} & -V^{-}_{d-} \\ V^{-}_{d-} & V^{-}_{q-} & V^{+}_{d+} & V^{+}_{q+} \\ V^{-}_{q-} & -V^{-}_{d-} & -V^{+}_{q+} & V^{+}_{d+} \end{bmatrix}^{-1}\begin{bmatrix} P_0 \\ Q_0 \\ P_{\mathrm{r\,cos}2} \\ P_{\mathrm{r\,sin}2} \end{bmatrix}. \tag{18}$$

Once the current references are obtained and in order to avoid the use of band-trap filter for decomposing the positive- and negative-sequence components of the current, a new control scheme based on the stationary $\alpha\beta$ frame with multi-frequency proportional-resonant (MFPR) controller (Yuan *et al*., 2002; Hu and He, 2007) is constructed as shown in Fig.4. To sufficiently eliminate the steady-state error of multiple current harmonics, such as the 3rd and 5th harmonic components concerned, the MFPR regulator in the stationary $\alpha\beta$ frame should have the structure as depicted in Fig.5.

According to Fig.5, the transfer function of the current regulator can be represented as

$$C(s) = K_{i\mathrm{P}} + \frac{sK_{i\mathrm{I}}}{s^2+\omega_{\mathrm{p}}^2} + \frac{sK_{i\mathrm{I}}}{s^2+(3\omega_{\mathrm{p}})^2} + \frac{sK_{i\mathrm{I}}}{s^2+(5\omega_{\mathrm{p}})^2}, \tag{19}$$

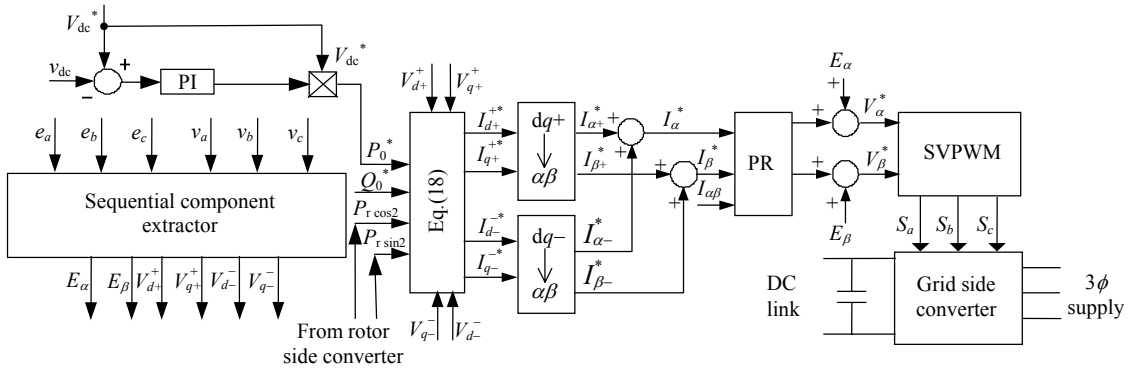

Fig.4 Schematic diagram of the proposed control system for grid-side PWM VSC

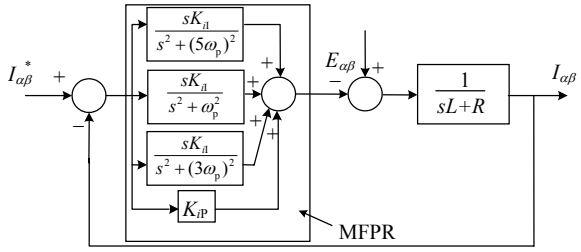

Fig.5 Current control diagram based on multi-frequency proportional resonant

where $K_{i\mathrm{P}}$ and $K_{i\mathrm{I}}$ are the proportional and resonant coefficients, which can be determined based on Naslin polynomial, $\omega_{\mathrm{p}}=100\pi$ is the grid angular frequency.

Rotor-side VSC control

According to Eq.(12), there are four rotor current components $I^{+}_{\mathrm{r}d+}$, $I^{+}_{\mathrm{r}q+}$, $I^{-}_{\mathrm{r}d-}$, $I^{-}_{\mathrm{r}q-}$ required to be controlled under unbalanced grid voltage conditions. In addition to independently controlling the average DC components of the active and reactive powers $P_{\mathrm{s}0}$ and $Q_{\mathrm{s}0}$, two more other subjects can be controlled. In this paper, the control system is to be designed to operate with either of the following control aims:

Target I: No rotor current oscillation, i.e. no rotor negative-sequence current;

Target II: Balanced stator current, which ensures balanced heating in the three-phase stator windings.

For target I, there are $I^{-*}_{\mathrm{r}d-}=0$ and $I^{-*}_{\mathrm{r}q-}=0$ and according to Eq.(12), the reference values of the positive- and negative-sequence rotor currents can be determined as

$$\begin{bmatrix} I^{+*}_{\mathrm{r}d+} \\ I^{+*}_{\mathrm{r}q+} \end{bmatrix} = \frac{2}{3}\frac{L_{\mathrm{s}}}{L_{\mathrm{m}}}\boldsymbol{M}^{-1}\left(\begin{bmatrix} P_{\mathrm{s}0} \\ Q_{\mathrm{s}0} \end{bmatrix} + \frac{3}{2}\frac{1}{L_{\mathrm{s}}}\boldsymbol{N}\begin{bmatrix} \psi^{+}_{\mathrm{s}d+} \\ \psi^{+}_{\mathrm{s}q+} \\ \psi^{-}_{\mathrm{s}d-} \\ \psi^{-}_{\mathrm{s}q-} \end{bmatrix} \right), \quad (20)$$

where

$$\boldsymbol{M}=\begin{bmatrix} V^{+}_{\mathrm{s}d+} & V^{+}_{\mathrm{s}q+} \\ V^{+}_{\mathrm{s}q+} & -V^{+}_{\mathrm{s}d+} \end{bmatrix},\ \boldsymbol{N}=\begin{bmatrix} V^{+}_{\mathrm{s}d+} & V^{+}_{\mathrm{s}q+} & V^{-}_{\mathrm{s}d-} & V^{-}_{\mathrm{s}q-} \\ V^{+}_{\mathrm{s}q+} & -V^{+}_{\mathrm{s}d+} & V^{-}_{\mathrm{s}q-} & -V^{-}_{\mathrm{s}d-} \end{bmatrix}.$$

While for Target II, the balanced stator current means $I^{-}_{\mathrm{s}d-}=I^{-}_{\mathrm{s}q-}=0$. According to Eq.(8), the reference values of the negative-sequence rotor currents can be expressed as

$$I^{-*}_{\mathrm{r}d-}=\psi^{-}_{\mathrm{s}d-}/L_{\mathrm{m}},\quad I^{-*}_{\mathrm{r}q-}=\psi^{-}_{\mathrm{s}q-}/L_{\mathrm{m}}. \quad (21)$$

According to Eq.(12), the reference values of the positive-sequence rotor currents can be calculated by

$$\begin{bmatrix} I^{+*}_{\mathrm{r}d+} \\ I^{+*}_{\mathrm{r}q+} \end{bmatrix} = \boldsymbol{M}^{-1}\left(\frac{2}{3}\frac{L_{\mathrm{s}}}{L_{\mathrm{m}}}\left(\begin{bmatrix} P_{\mathrm{s}0} \\ Q_{\mathrm{s}0} \end{bmatrix} + \frac{3}{2}\frac{1}{L_{\mathrm{s}}}\boldsymbol{N}\begin{bmatrix} \psi^{+}_{\mathrm{s}d+} \\ \psi^{+}_{\mathrm{s}q+} \\ \psi^{-}_{\mathrm{s}d-} \\ \psi^{-}_{\mathrm{s}q-} \end{bmatrix} \right) - \frac{1}{L_{\mathrm{m}}}\begin{bmatrix} V^{-}_{\mathrm{s}d-} & V^{-}_{\mathrm{s}q-} \\ V^{-}_{\mathrm{s}q-} & -V^{-}_{\mathrm{s}d-} \end{bmatrix}\begin{bmatrix} \psi^{-}_{\mathrm{s}d-} \\ \psi^{-}_{\mathrm{s}q-} \end{bmatrix} \right), \quad (22)$$

Once the reference rotor currents are obtained according to the individual control aim, $I^{+}_{\mathrm{r}d+}$, $I^{+}_{\mathrm{r}q+}$, $I^{-}_{\mathrm{r}d-}$, $I^{-}_{\mathrm{r}q-}$ are required to be regulated to follow their varying references, respectively. Similar to balanced control system (Hu and He, 2006) and according

to the rotor voltage equations in the positive- and negative-synchronously rotating frames, two rotor current controllers can be designed as

$$\begin{bmatrix} V_{rd+}^{+} \\ V_{rq+}^{+} \end{bmatrix} = \sigma L_r \begin{bmatrix} U_{rd+}^{+} \\ U_{rq+}^{+} \end{bmatrix} - \sigma L_r \boldsymbol{A}^{+} \begin{bmatrix} I_{rd+}^{+} \\ I_{rq+}^{+} \end{bmatrix} - \omega_{slip+} \frac{L_m}{L_s} \begin{bmatrix} \psi_{sq+}^{+} \\ -\psi_{sd+}^{+} \end{bmatrix}, \tag{23a}$$

$$\begin{bmatrix} V_{rd-}^{-} \\ V_{rq-}^{-} \end{bmatrix} = \sigma L_r \begin{bmatrix} U_{rd-}^{-} \\ U_{rq-}^{-} \end{bmatrix} - \sigma L_r \boldsymbol{A}^{-} \begin{bmatrix} I_{rd-}^{-} \\ I_{rq-}^{-} \end{bmatrix} - \omega_{slip-} \frac{L_m}{L_s} \begin{bmatrix} \psi_{sq-}^{-} \\ -\psi_{sd-}^{-} \end{bmatrix}, \tag{23b}$$

where

$$\boldsymbol{A}^{+} = \begin{bmatrix} -R_r/(\sigma L_r) & \omega_{slip+} \\ -\omega_{slip+} & -R_r/(\sigma L_r) \end{bmatrix},$$

$$\boldsymbol{A}^{-} = \begin{bmatrix} -R_r/(\sigma L_r) & \omega_{slip-} \\ -\omega_{slip-} & -R_r/(\sigma L_r) \end{bmatrix},$$

and $U_{rd+}^{+}, U_{rq+}^{+}, U_{rd-}^{-}, U_{rq-}^{-}$ are expressed as

$$\begin{cases} U_{rd+}^{+} = k_{pI1}(I_{rd+}^{+*} - I_{rd+}^{+}) + k_{iI1}\int (I_{rd+}^{+*} - I_{rd+}^{+})\mathrm{d}t, \\ U_{rq+}^{+} = k_{pI1}(I_{rd+}^{+*} - I_{rd+}^{+}) + k_{iI1}\int (I_{rq+}^{+*} - I_{rq+}^{+})\mathrm{d}t, \end{cases} \tag{24a}$$

$$\begin{cases} U_{rd-}^{-} = k_{pI2}(I_{rd-}^{-*} - I_{rd-}^{-}) + k_{iI2}\int (I_{rd-}^{-*} - I_{rd-}^{-})\mathrm{d}t, \\ U_{rq-}^{-} = k_{pI2}(I_{rd-}^{-*} - I_{rd-}^{-}) + k_{iI2}\int (I_{rq-}^{-*} - I_{rq-}^{-})\mathrm{d}t, \end{cases} \tag{24b}$$

where k_{pI1}, k_{iI1} and k_{pI2}, k_{iI2} are the proportional and integral coefficients of the positive- and negative-sequence current controllers, respectively.

Based on the aforementioned control strategies, an unbalanced control scheme for the wind-turbine driven DFIG under unbalanced grid supply voltage conditions was constructed, as shown in Fig.6. In this figure, a phase-locked loop (PLL) circuit is used to detect the grid voltage frequency and to follow the grid phase, which provides dependency for implementing positive- and negative-synchronously rotating transformations on stator and rotor voltages and currents. Besides, as shown in Eq.(6), the positive-sequence components appear in the dq^{+} reference frame as DC values, whereas, the negative-sequence components behave as oscillating quantities with frequency of $2\omega_s$. It is similar to the dq^{-} reference frame. In order to decompose the positive- and negative-sequence components, a notch filter tuned at $2\omega_s$ is employed to remove the oscillating items.

SIMULATION

Simulations of the proposed control strategies for a BTB PWM VSC used in DFIG-based wind power generation system were conducted using Matlab/Simulink. The DFIG is rated at 1.5 MW and its parameters are listed in Table 1. The nominal DC-link voltage was set at 1200 V and the switching frequencies for both converters were 3 kHz. During the simulations, the stator voltage was around 2% steady-state and 5% transient unbalances and the generator speed was fixed at 1.2 p.u.

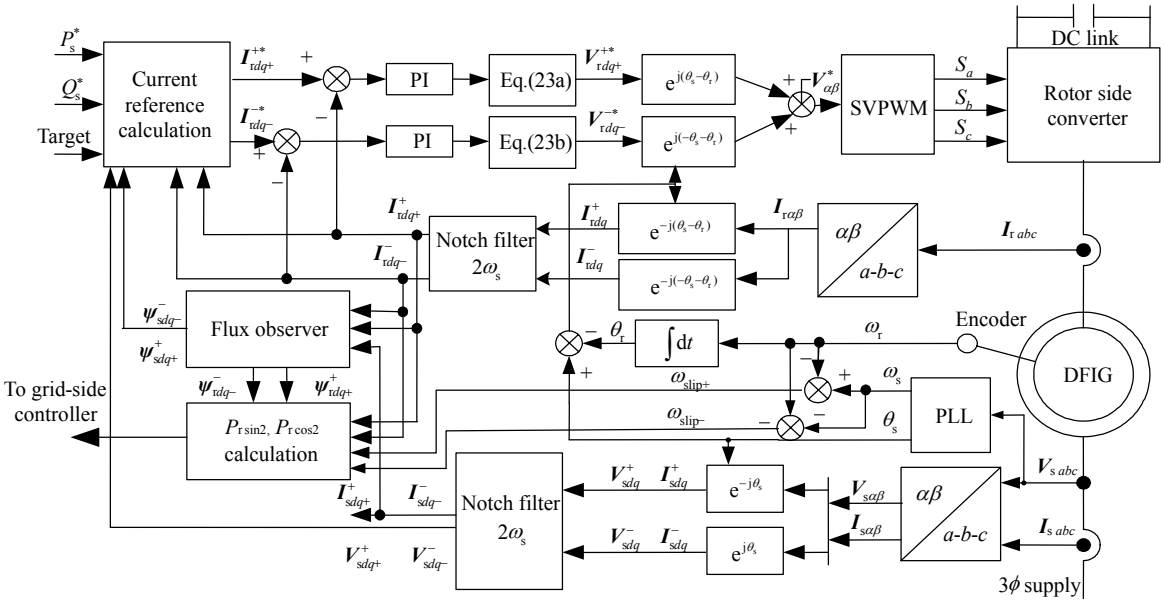

Fig.6 Schematic diagram of the proposed unbalanced control strategies for rotor-side PWM VSC under generalized unbalanced grid voltage conditions

As shown in Fig.7c, with the traditional balanced control (Hu and He, 2006) employed, the stator current becomes highly unbalanced in the presence of unbalanced stator voltage. The three-phase rotor currents, with frequencies equal to the rotor mechanical frequency minus the stator frequency, are made up of both the fundamental component of 10 Hz (60–50) and the harmonic component of 110 Hz (60 +50). The measured stator current unbalance is about 6.7% and the amplitude of the rotor current harmonics of 110 Hz is about 5.6% of the fundamental component of 10 Hz. Since the active power exchange between the DFIG rotor and the rotor-side VSC contains 100 Hz oscillation, the voltage ripples with 100 Hz in frequency and about 12.7 V in amplitude (peak-to-peak) appear in the DC link, which make the 3rd (150 Hz) harmonics of the grid-side VSC current be 4.2 % of the fundamental frequency. With the conventional grid-side VSC control design (Stankovic and Lipo, 2001) and the proposed rotor-side control strategy (Target I) employed, Fig.7b shows the simulated results with the same condition as in Fig.7c, from which it is obvious that the stator and rotor current unbalances are both impressed down to 1.8% and 0.6%, respectively, while the grid-side VSC still contains 4.8% of 150 Hz harmonic and the amplitude of DC-link voltage ripples are maintained at the value of 15.4 V. In Fig.7a, the simulated results predicted by employing the developed grid-side design and the

Table 1 Parameters of the simulated DFIG

Parameters	Values
Rated power	1.5 MW
Stator voltage	575 V
Stator/rotor turns ratio	0.38
Stator resistance R_s	0.00706 p.u.
Rotor resistance R_r	0.005 p.u.
Stator leakage inductance $L_{\sigma s}$	0.171 p.u.
Rotor leakage inductance $L_{\sigma r}$	0.156 p.u.
Mutual inductance L_m	2.9 p.u.
Lumped inertia const.	5.04 s

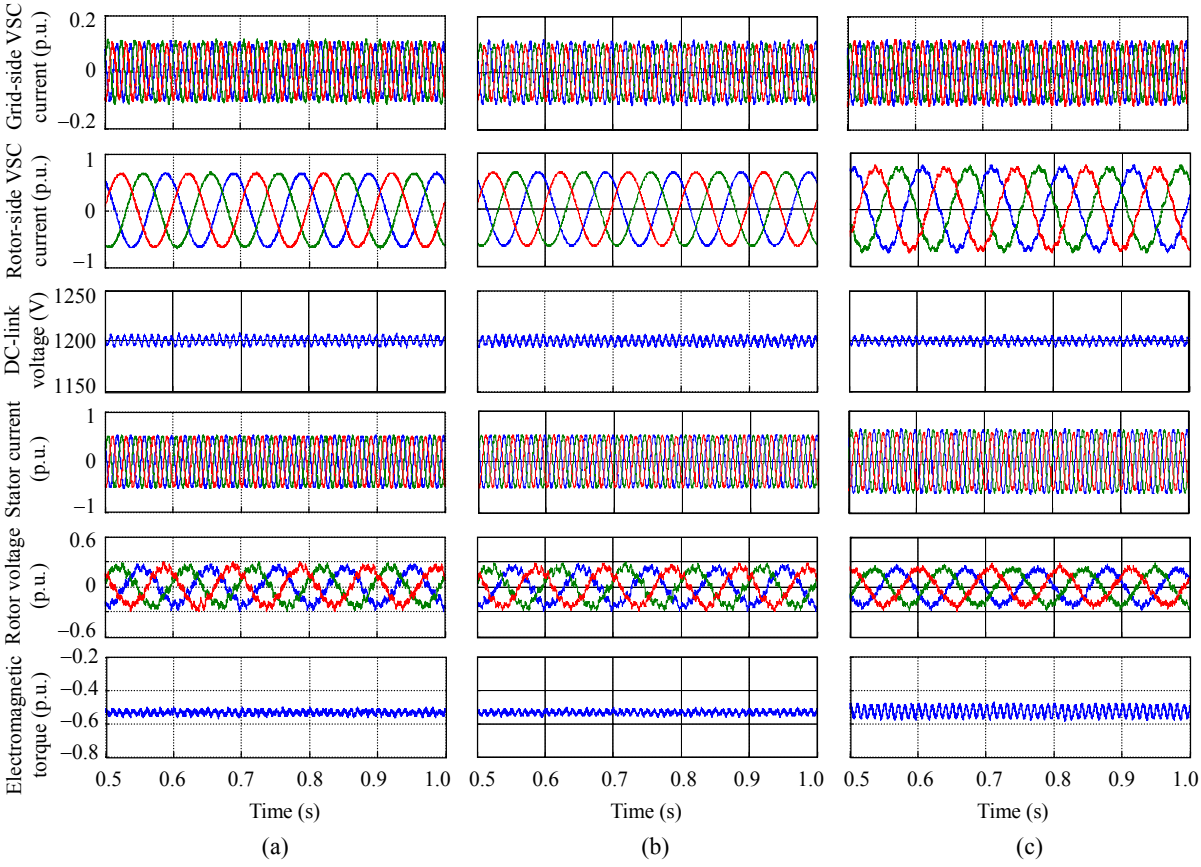

Fig.7 Simulated results under 2% stator voltage unbalance and ω_r=1.2 p.u.

(a) Proposed grid-side design+Proposed rotor-side design (Target I); (b) Traditional grid-side design+Proposed rotor-side design (Target I); (c) Balanced control design

proposed rotor-side control strategy (Target I) together are given. It is clear that the DC-link voltage ripples are effectively reduced to 10.5 V, and the associated grid-side current contains less than 2.8% of 150 Hz harmonic. Meanwhile, the stator and rotor current unbalances are even more diminished to 1.5% and 0.3%, respectively. It can be also concluded from Fig.7 that in order to control the rotor current precisely, the induced rotor voltage increases when grid voltage unbalance occurs. Meanwhile, the fluctuation at twice the grid frequency in the electromagnetic torque gets effectively diminished with the proposed control design for the rotor-side VSC. For comparison, the simulated results are summarized in Table 2, where $\boldsymbol{I}_g$ is the grid-side VSC current vector.

Further tests on the proposed grid-side VSC design and the two alternative rotor-side VSC control strategies were conducted with the same conditions except for 5% stator voltage unbalance as in Fig.7. The results are shown in Fig.8, where the control aim of the rotor-side VSC was initially set to Target I, and then changed to Target II at the instant of 0.5 second. As can be measured from Fig.8, with rotor-side VSC controller set to Target I, the rotor current unbalance is suppressed to only 0.11%, while the stator current unbalance is measured about 1.5%. When switched to Target II, the stator current unbalance becomes very low, only 0.2% with 1% unbalance of rotor current. Besides, with both rotor-side VSC control targets, the DC-link voltage ripples are well diminished to 21.5 V

Table 2 Comparative results with different control strategies employed under unbalanced grid-voltage conditions

	$\boldsymbol{I}_s$ unbalance (%)	$\boldsymbol{I}_r$ 11th (110 Hz) unbalance (%)	$\boldsymbol{I}_g$ 3rd (150 Hz) harmonics (%)	V_{dc} ripple (V)
Fig.7a	1.5	0.11	2.8	10.5
Fig.7b	1.7	0.3	4.8	15.4
Fig.7c	6.7	5.6	4.2	12.7

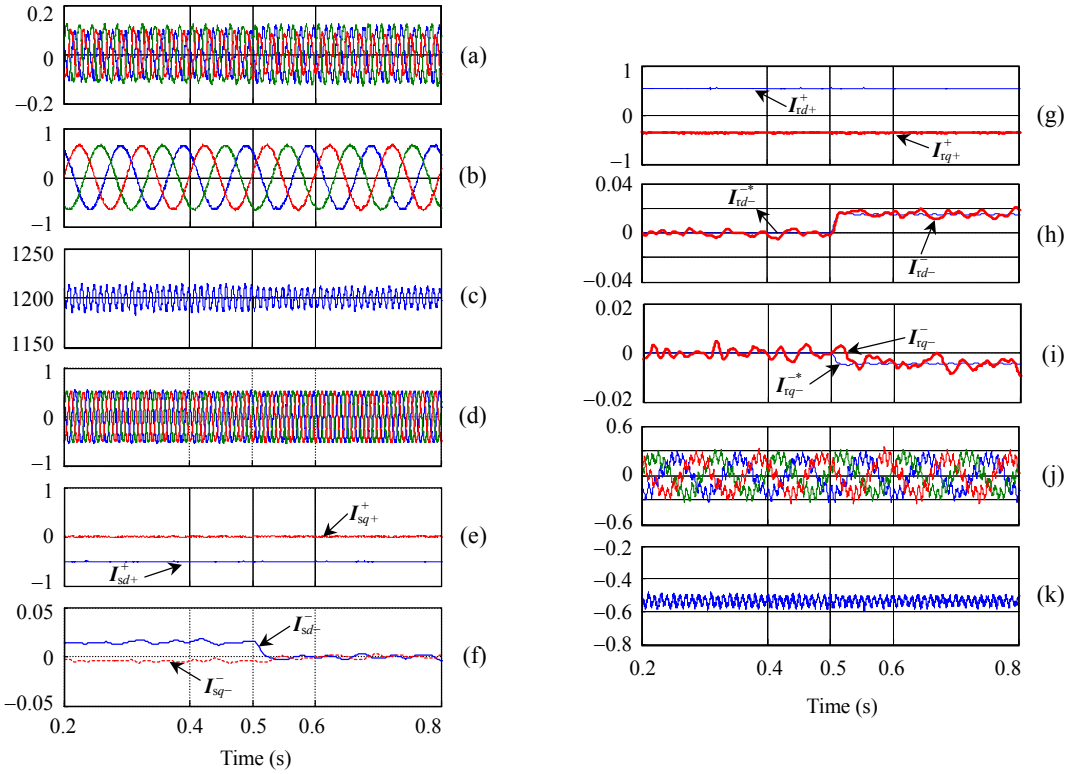

Fig.8 Simulated results during 5% stator voltage unbalance with the proposed grid-side control design and two alternatively proposed rotor-side control strategies: Target I (0.2~0.5 s), Target II (0.5~0.8 s)

(a) Three-phase grid-side VSC current (p.u.); (b) Three-phase rotor-side VSC current (p.u.); (c) DC-link voltage (V); (d) Three-phase stator current (p.u.); (e) Stator positive-sequence *dq* current (p.u.); (f) Stator negative-sequence *dq* current (p.u.); (g) Rotor positive-sequence *dq* current (p.u.); (h) Rotor negative-sequence *d* current (p.u.); (i) Rotor negative-sequence *q* current (p.u.); (j) Three-phase rotor voltage (p.u.); (k) Electromagnetic torque (p.u.)

in peak-to-peak amplitude. It is easily concluded from Fig.8 that as a result of well-regulated positive- and negative-rotor currents in the positive- and negative-synchronously rotating reference frames, the alternative control strategies proposed could be fully achieved and the system performance is sufficiently satisfied.

CONCLUSION

This paper has presented an analysis and control in detail for a BTB PWM VSC, used in the DFIG-based wind power generation system, operating under unbalanced grid voltage conditions. The following conclusions can be made:

(1) Under unbalanced grid-voltage conditions, the developed unified mathematical model of DFIG in the positive- and negative-synchronously rotating frames provides a useful tool for defining exactly the stator and rotor instantaneous active and reactive powers, which indicates that significant oscillations of twice the grid frequency do exist.

(2) The modified control design for grid-side VSC takes into consideration the oscillating power-flow exchanging between the DFIG rotor and the rotor-side converter under unbalanced grid voltage conditions, which diminishes the amplitude of the DC-link voltage ripples of twice the grid frequency and leads to the possibility of reducing the size of DC-link capacitor for a BTB PWM VSC used in a DFIG-based wind-power generation system during unbalanced network supply.

(3) With the proposed design employed to control the grid-side VSC, a rotor current control scheme based on the positive- and negative-synchronously rotating reference frames was proposed to provide precise control of the rotor currents. As a result, the two alternatively proposed control targets for rotor-side VSC were achieved satisfactorily, which enhances the unbalanced FRT capability of DFIG-based wind-power generation systems under unbalanced network supply voltage. Meanwhile, the induced rotor voltage gets increased so as to provide the precise rotor current control, but it will not increase the above DC-link voltage of the converters under the aforementioned voltage unbalance.

References

Hu, J.B., He, Y.K., 2006. Dynamic modeling and robust current control of wind-turbine used DFIG during AC voltage dip. *J. Zhejiang Univ. Sci. A*, **7**(10):1757-1764. [doi:10.1631/jzus.2006.A1757]

Hu, J.B., He, Y.K., 2007. Modeling and control of grid-connected voltage sourced converter under generalized unbalanced operation conditions. Submitted to *IEEE Trans. on Energy Conv.*, under review.

Idsoe Nass, B., Undeland, T., Gjengedal, T., 2002. Methods for Reduction of Voltage Unbalance in Weak Grids Connected to Wind Plants. IEEE Workshop on Wind Power and the Impacts on Power Systems. Norway.

Morren, J., de Haan, S.W.H., Bauser, P., Pierik, J.T.G., 2003. Comparison of Complete and Reduced Models of a Wind Turbine Using Doubly-Fed Induction Generator. Proc. 10th European Conference on Power Electronics and Applications. Toulouse.

Morren, J., de Haan, S.W.H., 2005. Ride-through of wind turbines with doubly-fed induction generator during a voltage dip. *IEEE Trans. on Energy Conv.*, **20**(2):435-441. [doi:10.1109/TEC.2005.845526]

National Grid Transco, 2004. Appendix 1: Extracts from the Grid Code-Connection Conditions. Http://www.national-grid.com

Pena, R., Clare, J.C., Asher, G.M., 1996. Doubly fed induction generator using back-to-back PWM converter and its application to variable-speed wind-energy generation. *IEE Proc. B*, **143**(3):231-241.

Petersson, A., Harnefors, L., Thiringer, T., 2005. Evaluation of current control methods for wind turbines using doubly-fed induction machines. *IEEE Trans. on Power Elect.*, **20**(1):227-235. [doi:10.1109/TPEL.2004.839785]

Stankovic, A.V., Lipo, T.A., 2001. A novel control method for input output harmonic elimination of the PWM boost type rectifier under unbalanced operating conditions. *IEEE Trans. on Power Elect.*, **16**(5):603-611. [doi:10.1109/63.949493]

Sun, T., Chen, Z., Blaabjerg, F., 2005. Transient stability of DFIG wind turbines at an external short-circuit fault. *Wind Energy*, **8**(3):345-360. [doi:10.1002/we.164]

Tapia, A., Tapia, G., Ostolaza, J.X., Saenz, J.R., 2003. Modeling and control of a wind turbine driven doubly fed induction generator. *IEEE Trans. on Energy Conv.*, **18**(2):194-204. [doi:10.1109/TEC.2003.811727]

Xu, L., Andersen, B.R., Cartwright, P., 2005. VSC transmission operating under unbalanced AC conditions-analysis and control design. *IEEE Trans. on Power Del.*, **20**(1):427-434. [doi:10.1109/TPWRD.2004.835032]

Yazdani, A., Iravani, R., 2006. A unified dynamic model and control for the voltage-sourced converter under unbalanced grid conditions. *IEEE Trans. on Power Del.*, **21**(3):1620-1629. [doi:10.1109/TPWRD.2006.874641]

Yuan, X., Merk, W., Stemmler, H., Allmeling, J., 2002. Stationary-frame generalized integrators for current control of active power filters with zero steady-state error for current harmonics of concern current under unbalanced and distorted operating conditions. *IEEE Trans. on Ind. Appl.*, **38**(2):523-532. [doi:10.1109/28.993175]